Measurement Report: Rapid decline of aerosol absorption coefficient and aerosol optical properties effects on radiative forcing in an urban area of Beijing from 2018 to 2021

Xinyao Hu[1,2], Junying Sun[1,3*], Can Xia[1,4], Xiaojing Shen[1], Yangmei Zhang[1], Quan Liu[1], Zhaodong Liu[1,4], Sinan Zhang[1], Jialing Wang[1], Aoyuan Yu[1,2], Jiayuan Lu[1], Shuo Liu[1], and Xiaoye Zhang[1]

[1]State Key Laboratory of Severe Weather & Key Laboratory of Atmospheric Chemistry of CMA, Chinese Academy of Meteorological Sciences, Beijing 100081, China

[2]University of Chinese Academy of Sciences, Beijing 100049, China

[3]State Key Laboratory of Cryospheric Science, Northwest Institute of Eco-Environment and Resources, Chinese Academy of Sciences, Lanzhou 730000, China

[4]Nanjing University of Information Science & Technology, Nanjing 210044, China

**Correspondence to*: Junying Sun (jysun@cma.gov.cn)

Abstract

Reliable observations of aerosol optical properties are crucial for quantifying the radiative forcing of climate. The simultaneous measurements of aerosol optical properties at three wavelengths for PM_1 and PM_{10} were conducted in urban Beijing from March 2018 to February 2022. The aerosol absorption coefficient (σ_{ab}) at 550 nm of PM_{10} and PM_1 decreased by 55.0% and 53.5% from 2018 to 2021. Significant reduction in σ_{ab} may be related to reduced primary emissions caused by effective air pollution control measures.

$PM_{2.5}$ mass concentration decreased by 34.4% from 2018 to 2021. SSA increased from 0.89 ± 0.04 for PM_{10} (0.87 ± 0.05 for PM_1) in 2018 to 0.93 ± 0.03 for PM_{10} (0.91 ± 0.04 for PM_1) in 2021. Increasing SSA and decreasing $PM_{2.5}$ mass concentration suggest that the fraction of absorbing aerosols decreased with improved air quality due to pollution control measure-taking. The annual average submicron absorption ratio (Rab) increased from 86.1% in 2018 to 89.2% in 2021, suggesting that fine particles are the main contributors to total PM_{10} absorption and that the fine particles to absorption became more important. Absorption Angstrom exponent (AAE) in winter decreased from 2018 to 2021, implying a decreasing contribution from brown carbon to light absorption, which may relate to the reduced emissions of biomass burning and coal combustion. During the study period, aerosol radiative forcing efficiency became more negative mainly influenced by increasing SSA, and was −27.0 and -26.2 W m^{-2} AOD^{-1} for PM_{10} and PM_1 in 2021. Higher σ_{ab} and $PM_{2.5}$ mass concentrations were primarily distributed in clusters 4 and 5, transported from the south and the west of Beijing each year. σ_{ab} and $PM_{2.5}$ corresponding to clusters 4 and 5 decreased evidently from 2018 to 2021, which may result from the control of source emissions in surrounding regions of Beijing. The 4-year data presented in this study provide critical optical parameters for radiative forcing assessment within two size ranges and are helpful for evaluating the effectiveness of clean air action.

1 Introduction

Atmospheric aerosols perturb the Earth's atmospheric radiation balance and climate forcing by directly affecting the scattering and absorption of solar radiation (Charlson et al., 1992; Jacobson, 2001) but also indirectly affecting cloud reflectivity and precipitation

processes (Twomey, 2007). Light-scattering aerosols contribute to offsetting the warming effect of CO_2, while absorbing aerosols contribute to the heating of the atmosphere (Bond and Bergstrom, 2007), and produce a positive radiative forcing (Segura et al., 2016). The largest contribution to aerosol absorption is from black carbon (BC), which absorbs strongly over the entire solar spectrum (Bond and Bergstrom, 2007). Dust and brown carbon (BrC) are also light absorption aerosols, which strongly absorb in the ultraviolet (UV) spectrum. Globally, aerosols contributed an effective radiative forcing (ERF) of –1.3 ± 0.7 W m^{-2}, and the ERF due to emissions of BC is now estimated to be 0.11 (–0.20 to 0.42) W/m^2 between 1750 to 2019 (Szopa et al., 2021). However, aerosol properties are highly spatial and temporal variable, which results in radiative forcing variation from local to global scales and creates an observational challenge (Collaud Coen et al., 2013; Ealo et al., 2018; Andrews et al., 2011). Therefore, reliable observations of aerosol optical properties are crucial for quantifying the radiative forcing of climate.

In order to assess the role of aerosols on climate forcing accurately, a set of parameters that describe aerosol's optical properties are needed, such as scattering coefficient (σ_{sp}), absorption coefficient(σ_{ab}), backscatter fraction(b) and single scattering albedo (SSA). SSA is a key variable that determines the magnitude and the sign of the aerosol forcing (J. Hansen et al., 1997; Lee et al., 2007; Li et al., 2022a; Zhang et al., 2020). Previous studies found that SSA values range from slightly less than 0.8 to almost purely scattering particles with SSA close to 1 at worldwide locations (Laj et al., 2020; Pandolfi et al., 2018), and higher SSA values indicate a tendency towards a cooling effect (Li et al., 2022a). The backscatter fraction (b) describes how much aerosol particles scatter radiation in the backward hemisphere compared with the total scattering, which is a crucial variable for

aerosol radiative forcing efficiency (RFE) calculations (Andrews et al., 2011; Sheridan and Ogren, 1999; Luoma et al., 2019). Previous studies found that the magnitude of RFE increases with increasing b (Shen et al., 2018). Typical values of b for the atmospheric aerosol at 550 nm were from approximately 0.05 to 0.20 (Titos et al., 2021).

Besides, aerosol optical properties are wavelength-dependent, absorption Angstrom exponent (AAE) describes the spectral dependence of light absorption by aerosols and is typically used to differentiate between different aerosol types (Helin et al., 2021). The AAE for fresh BC is ~1, indicating "weak" spectral dependence of light absorption (Bond et al., 2013; Bond and Bergstrom, 2007), and the AAE >1 indicates the presence of BrC or dust, which tend to exhibit absorption that increases sharply as wavelength decreases (Moosmüller et al., 2009; Lack and Cappa, 2010). Thus, obtaining the aerosol absorption coefficient at different wavelengths is essential and can be helpful to differentiate between different aerosol types.

As one of the world's most populous and rapidly developing megacities, Beijing experienced rapid economic growth and urbanization, accompanied by severe air pollution. Many in-situ measurements of aerosol optical properties have been conducted in Beijing (Bergin et al., 2001; He et al., 2009; Garland et al., 2009; Jing et al., 2015; Wang et al., 2019; Zhao et al., 2019; Xia et al., 2020). Previous studies found that high aerosol loading leads to large σ_{ab} in Beijing (Jing et al., 2015; Garland et al., 2009; Bergin et al., 2001). Moreover, the AAE showed significant seasonal variations in Beijing. Significantly higher AAE in winter than in summer highlights the important role of absorption of non-BC components (e.g. BrC) in winter (Xie et al., 2020; Xia et al., 2020). In order to reduce emissions and improve air quality, the government implemented strict pollution control

measures (Xu and Zhang, 2020). Significant decreases in $PM_{2.5}$ mass concentrations were found in Beijing and the annual mean elemental carbon (EC) concentrations declined from 4.0 to 2.6 μg m^{-3} from March 2013 to February 2018 in Beijing (Ji et al., 2019). Xia et al. (2020) separated and quantified the effects of emission control and meteorological transport variability on BC loading from 2015 to 2017 in north China Plain. However, the environmental effects caused by emission controls are related to not only their mass concentrations, but also their optical properties and radiative effect (Luo et al., 2020). Therefore, it's necessary to investigate the multiple-year variations in aerosol optical properties and radiative effect in providing a comprehensive understanding of the effects of emission control. Wang et al. (2019) found that absorption coefficient (σ_{ap}) for $PM_{2.5}$ decreased from 2014 to 2017, with a significant decrease of σ_{ap} in autumn. Sun et al. (2022) estimated that the direct radiative forcing of BC decreased by 67% from +3.36Wm^{-2} in 2012 to +1.09 Wm^{-2} in 2020. However, these studies were mostly conducted with conventional total suspended particulate (TSP) cyclone, $PM_{2.5}$ size cut, or PM_{10} size cut. Few studies focused on the sub-micron and super-micron particle optical properties and estimated aerosol radiative effect in the post-"Action Plan on Prevention and Control of Air Pollution" era. Acquiring the aerosol optical for the total (< 10μm diameter) and submicron aerosol is also in line with the aerosol advisory group of the Global Atmosphere Watch recommendation (WMO/GAW, 2016).

In this study, the simultaneous measurements of aerosol optical properties at three wavelengths for PM_1 and PM_{10} were conducted in urban Beijing from March 2018 to February 2022. The annual, seasonal, and diurnal variations of aerosol optical properties for two size cuts were investigated. The scattering properties of aerosols for two size ranges

(PM$_{10}$ and PM$_1$) under dry conditions observed in Beijing have been analyzed in detail by Hu et al. (2021). Thus, this study mainly focused on the variation of aerosol absorption coefficient, single scattering albedo, and absorption Angstrom Exponent for PM$_{10}$ and PM$_1$. Moreover, the aerosol radiative effects in two size cuts were estimated. Finally, the transport and its impact on aerosol optical properties were analyzed. The 4-year data presented in this study provide key optical parameters for radiative forcing assessment within two size ranges and are helpful for evaluating the effectiveness of clean air action.

2 Instrumentation and methods

2.1 Site description

The sampling site in this study is located on the roof of the Chinese Academy of Meteorological Sciences (CAMS, 116°19′ E, 39°57′ N, 46 m a.s.l) in Beijing, which is a typical urban site in the northwest of Beijing between the 2nd and 3rd ring roads. The laboratory is on the roof of CAMS building, and the measurements are taken at 53 m above ground level. The site is mainly influenced by local emissions from residential living and traffic pollution (Xia et al., 2019).

2.2 Instruments and measurements

The ambient air was sampled into a PM$_{10}$ impactor with 16.7 LPM and then to an adsorption aerosol dryer, which controlled the relative humidity (RH) of sample air below 30% (Tuch et al., 2009). The dried aerosol sample passes through switched impactors that toggle the aerosol size cut between 1.0 μm (<1 μm) and 10 μm (<10 μm) aerodynamic particle diameters every 30 min, thus allowing to measure both fine and coarse particles

(Hu et al., 2021). The sample aerosol was then passed into the Nephelometer (TSI Inc., Model 3563) and Tricolor Absorption Photometer (TAP, Brechtel Manufacturing, Inc., Hayward, CA, USA).

The integrating nephelometer measured the scattering coefficient (σ_{sp}) (angular range of 7–170°) and backscattering coefficient (σ_{bsp}) (angular range of 90–170°) at 450, 550, and 700 nm. The scattering and backscattering coefficient were corrected for truncation and instrument non-idealities using the method described by Anderson and Ogren (1998). Details are given in Hu et al. (2021). To ensure the data's accuracy and reliability, the nephelometer was calibrated regularly using filtered ambient air using a HEPA filter and CO_2 with a purity of 99.999%. A zero-check was automatically performed once per hour to obtain a nephelometer background.

TAP measures absorption coefficient (σ_{ab}) at 465, 520, and 640 nm with the 47 mm diameter, glass-fiber filter and is a commercially available version of the continuous light absorption photometer (CLAP), which is low cost and high sensitivity (Ogren et al., 2017). The TAP comprises eight sample spots and two reference spots. The aerosol-laden air passes through one sample spot at a time, which allows for 8 times the filter lifetime compared to single-spot photometers (Davies et al., 2019). Unlike the Multi-Angle Absorption Photometer (MAAP), TAP does require a co-located aerosol light scattering or extinction measurement to derive aerosol light absorption (Ogren et al., 2017). Thus, simultaneous observation of aerosol light scattering has been measured and used to correct absorption data. When the Nephelometer and TAP were calibrated or malfunctioning, no data are available. During this study, 84% of the data was effective.

2.3. Data processing

The TAP measures the light transmitted through a filter as particles are deposited onto the filter. The filter attenuation coefficient (σ_{atn}), at a specific wavelength (λ), can be determined as:

$$\sigma_{atn}(\lambda)=\frac{A}{Q}\times\frac{\Delta atn(\lambda)}{\Delta t} \quad (1)$$

where Δatn (λ) is the filter attenuation at times t1 and t2, A is the area of on the filter, and Q is the sample flow rate through the filter.

In order to correct the error caused by multiple scattering and filter loading, the aerosol light absorption coefficient (σ_{ab} (λ)) was corrected based on the methods of Bond et al. (1999) and Ogren et al. (2017). First, the effect of filter loading was calibrated based on Eq. (2):

$$\sigma_{ab}(\lambda)\_raw=\frac{0.85\times\sigma_{atn}(\lambda)}{K_2\times(1.0796\times Tr(\lambda)+0.71)} \quad (2)$$

Then, σ_{ab} (λ)_raw at 465, 520, and 640 nm were adjusted to the wavelength of the light scattering coefficient based on the calculated AAE. Finally, the multiple scattering effect was corrected based on Eq. (3):

$$\sigma_{ab}(\lambda)=\sigma_{ab}(\lambda)\_raw-\frac{K_1\times\sigma_{sp}(\lambda)}{K_2} \quad (3)$$

where Tr (λ) is the normalized filter transmittance at time t relative to transmittance at the start of sampling (t =0) and σ_{sp} is the aerosol light-scattering coefficient at 450, 550, and 700 nm measured by the nephlometer. K_1 and K_2 were derived by Bond et al. (1999) as K_1 =0.02±0.02 and K_2 =1.22±0.20, where the uncertainties are given for the 95% confidence level.

Using the corrected absorption coefficient data, the following parameters were calculated:

Absorption Angstrom exponent (AAE) describes the spectral dependence of light absorption.

$$AAE = -\frac{\ln(\sigma_{ab}^{\lambda 1}/\sigma_{ab}^{\lambda 2})}{\ln(\lambda 1/\lambda 2)} \quad (4)$$

The submicron absorption ratio (Rab) is determined as the ratio of the absorption coefficients for PM_1 and PM_{10}.

$$Rab = \frac{\sigma_{ab}(D<1\mu m)}{\sigma_{ab}(D<10\mu m)} \quad (5)$$

where σ_{ab} (D<1 μm) and σ_{ab} (D<10 μm) are σ_{ab} for particle diameters <1 μm and 10 μm, respectively.

Aerosol radiative forcing efficiency (RFE) at top-of-the-atmosphere (TOA) is a simplified formula that describes how large of an impact the aerosols would make to the aerosol radiative forcing (ΔF) per unit of aerosol optical depth (AOD) (Sheridan and Ogren, 1999) and we estimated the RFE at TOA as the Eq.6 (Haywood and Shine, 1995; Sheridan and Ogren, 1999):

$$RFE = \frac{\Delta F}{AOD} = -DS_0T_{at}^2(1-A_C)\times SSA\times\beta\times((1-R_s)^2-(\frac{2R_S}{\beta})\times(\frac{1}{SSA}-1)) \quad (6)$$

where D is the fractional day length, S_0 is the solar constant, T_{at} is the atmospheric transmission, Ac is the fractional cloud amount, and Rs is the surface reflectance. The constants used were D = 0.5, So = 1370 Wm^{-2}, T_{at} = 0.76, Ac = 0.6, and Rs = 0.15 as suggested by Haywood and Shine (1995), and upper scatter fraction β was calculated from $\beta = 0.0817+1.8495\times b-2.9682\times b^2$. backscatter fraction (b) was calculated based on scattering coefficient (σ_{sp}) and backscattering coefficient (σ_{bsp}) measured by Nephelometer

as $b = \sigma_{bsp}/ \sigma_{sp}$. Equation (6) has been widely used to assess the intrinsic radiative forcing efficiency of aerosols at the top of the atmosphere (Sheridan and Ogren, 1999; Virkkula et al., 2011; Shen et al., 2018). Note that RFE in this study was in a dry condition. As the backscatter fraction and single scattering albedo are all RH-dependent, the RFE is also sensitive to RH (Fierz-Schmidhauser et al., 2010). Previous studies revealed that RFE increased as the elevating RH (Titos et al., 2021; Xia et al., 2023). In this study, the values of ΔF at TOA were also caculated by multiplying the RFE for PM_{10} with the AOD of ambient atmospheric aerosols observed at the CAMS site during the study periods. AOD can be downloaded from Aerosol Robotic Network (AERONET). Note that RFE was at a dry state, thus the ΔF at TOA here may be slightly underestimated.

2.4. Other data used

The hourly $PM_{2.5}$ and PM_{10} mass concentrations were measured at Guan yuan station, which is about 3km from the CAMS site. The data can be derived from the national air quality real-time publishing platform (http://106.37.208.233:20035/). The hourly meteorological data were measured at Haidian station (station No. 54399) and obtained from the National Meteorological Information Center of China Meteorological Administration.

2.5. Back trajectories analysis

To investigate the influence of air mass origins on aerosol optical properties, 48-h backward trajectories arriving at Beijing at a height of 500 m above ground level were calculated from 0:00 to 23:00 local time each day from March 2018 to February 2022,

using the Trajstat Software, combined with HYSPLIT 4 model (Hybrid Single-Particle Lagrangian Integrated Trajectory), and the NCEP Global Data Assimilation System (GDAS) data with a 1° × 1° resolution (Draxler and Hess, 1998; Wang et al., 2009).

In this study, four seasons are defined as follows: spring from March to May, summer from June to August, autumn from September to November, and winter from December to the following February, and all data are reported in Beijing time (UTC+8).

3 Results and discussion

3.1 Temporal variation of aerosol optical properties

Figure 1 shows the annual variation of σ_{ab}, SSA, Rab, and $PM_{2.5}$ mass concentration from 2018 to 2021. During the study period, the annual mean $PM_{2.5}$ in 2018 was 54.7 μg m^{-3}, and it decreased by 34.4% (35.9 μg m^{-3}) in 2021, which suggested that the strict pollution control measures are effective in reducing the PM loadings in Beijing (Lei et al., 2021). Gong et al. (2022) demonstrated that emission reduction dominated the variations of $PM_{2.5}$ mass concentration in Beijing from 2013 to 2020, and meteorology and emission reduction contributed 7% and 63.2% of decreases, respectively. σ_{ab} at 550 nm of PM_{10} and PM_1 showed similar annual variations. The annual mean σ_{ab} at 550 nm of PM_{10} and PM_1 decreased by 55.0% and 53.5%, respectively, from 2018 to 2021. The Mann–Kendall trend test supported that the decrease in σ_{ab} for PM_1 and PM_{10} from 2018 to 2021 was significant (Table S1). Carbonaceous aerosol, especially black carbon, is closely related to aerosol absorption (Yang et al., 2009). A continuous decrease in σ_{ab} was consistent with the continuous reduction of black carbon concentration observed in Beijing in previous studies (Ji et al., 2019; Sun et al., 2022), which was mainly related to significantly reduced primary

emissions caused by effective air pollution control measures in recent years (Xia et al., 2020). The annual mean σ_{ab} for PM_{10} and PM_1 in 2021 was 9.8 Mm^{-1} and 8.7 Mm^{-1}, which were both lower than the result observed in Nainital, in the GH region, India (Dumka et al., 2015), and the measurement at an urban site in Spain from March 2006 to February 2007 (Titos et al., 2012). In fact, with the emission reduction and improvement of air quality, the aerosol scattering coefficient (σ_{sp}) for PM_{10} and PM_1 also decreased in Beijing. Hu et al. (2021) revealed that σ_{sp} decreased by approximately 18.4% for PM_{10}, and 16.7% for PM_1 from 2018 to 2019 in Beijing. Atmospheric conditions also have an effect on aerosol optical properties. The variations of meteorological parameters from 2018 to 2021 (Figure S4) showed that pressure, wind speed, temperature, and RH varied slightly, while accumulated precipitation increased in 2021 compared with the other 3 years. On the other hand, a correlation analysis was made between aerosol optical properties and meteorological parameters. The Pearson correlation coefficients (R) between σ_{ab} and meteorological parameters (Table S2) are lower than 0.5, indicating that a weak correlation ($R<0.5$) was found between σ_{ab} and meteorological parameters. This suggests that the meteorological parameters' influence on σ_{ab} is minor. Xia et al. (2020) revealed that the effect of emission reduction was the major reason for the decrease of BC in Beijing. Actually, σ_{ab} that was observed at a background station in China and the European stations, which was with time series longer than 10 years, also observed the reduction. σ_{ab} showed a statistically significant decreasing trend in Mt.Waliguan, a background station in China, from 2008–2018 (Collaud Coen et al., 2020), which was similar to a decreasing trend of black carbon (BC) in Mt.Waliguan from 2008-2017, mainly related to emission reduction (Dai et al., 2021). A statistically significant decrease of 10-year σ_{ap} was found in 12 stations in Europe,

264 which was similar to a decreasing trend in BC concentration in Europe related primarily to
265 traffic emission decreases (Collaud Coen et al., 2020).

266 SSA is a key variable in assessing the aerosol radiative forcing. The variation of SSA
267 also reflects the the ratio of aerosol scattering to total extinction with aerosol composition
268 changes. The annual variations of SSA for PM_{10} and PM_1 were similar. During 2018-2021,
269 annual mean SSA at 550 nm increased from 0.89 ± 0.04 for PM_{10} (0.87 ± 0.05 for PM_1) in
270 2018 to 0.93 ± 0.03 for PM_{10} (0.91 ± 0.04 for PM_1) in 2021. Increasing SSA and decreasing
271 $PM_{2.5}$ mass concentration during the past four years suggested that the fraction of absorbing
272 aerosols became lower compared to scattering aerosols with the improvement of air quality
273 due to pollution control measure-taking. Collaud Coen et al. (2020) found that SSA
274 observed in Mt. Waliguan, a background station in Asia, presented an increasing trend
275 based on 10-year datasets, which were related to more recent abatement policies. The mean
276 submicron absorption ratio (Rab) increased yearly during the same period. It was from 86.1%
277 in 2018 to 89.2% in 2021, suggesting that fine particles are the main contributors to total
278 PM_{10} absorption, and the contributions from fine particles to absorption became more
279 important.

280 The σ_{ab}, SSA, and AAE for PM_1 and PM_{10} showed similar annual variations in all
281 seasons (Fig. 2 and Fig. S1). Thus, if not stated otherwise, the following discussion takes
282 the aerosol optical properties of PM_{10} as an example. As shown in Fig. 2 seasonal average
283 of σ_{ab} presented a continuous reduction during all seasons from 2018 to 2021, reflecting
284 the reduction of absorbing aerosols which were related to effective control of absorbing
285 aerosols emissions in Beijing. σ_{ab} decreased by half in autumn and winter during the study
286 period, which was probably due to reducing coal consumption as a heating source and the

reduction of biomass burning. Compared with 2018, σ_{ab} in the winter of 2019, 2020 and 2021 decreased by 3.0%, 24.9% and 53.2%, respectively. In the winter of 2019, the lockdown of COVID-19 caused emission reduction from human activities in China (Le et al., 2020; Tian et al., 2020), however, the unexpected smallest reduction of σ_{ab} was observed in the winter of 2019 compared with the winter of 2020 and 2021. This is related to the fact that severe haze pollution still occurred in the North China Plain and BC concentrations rose unexpectedly during the lockdown period (Liu et al., 2021; Jia et al., 2021). In particular, σ_{ab} for PM_1 and PM_{10} decreased even up to 63% and 67% in the summer from 2018 to 2021. Traffic is a relatively stable source of absorption aerosols in summer (Li et al., 2022b). The largest deduction of σ_{ab} was in summer and could be related to more strict vehicle emission standards (Zhang et al., 2019).

In general, AAE was lowest in summer and highest in winter. The mean values of AAE for PM_{10} were 1.13 and 1.41 in summer and winter, respectively, similar to result at an urban site in Beijing in 2018 (Xie et al., 2020). During summer, the average AAE was generally close to 1, which suggested that BC from traffic emissions was the major component of light-absorbing aerosols. Li et al. (2022b) found that the percentage of liquid fuel (traffic) contributing to the total BC was 86.8% in summer in Beijing. The highest AAE suggested that BrC contributed to light absorption strongest in winter, which is due to enhanced emissions from biomass burning and coal combustion in winter (Sun et al., 2018). Notably, AAE decreased in winter from 1.48 for PM_{10} (1.48 for PM_1) in 2018 to 1.37 for PM_{10} (1.34 for PM_1) in 2021 (Fig. 2 and Fig. S1), indicating a decreasing contribution from BrC to light absorption, which may relate to the effect control of biomass burning and coal combustion caused by changes in heating energy structure (Ji et al., 2022).

To improve air quality, the Beijing-Tianjin-Hebei region adjusted the energy structure during the heating period and developed clean heating projects, such as the “coal to gas” project (Zhao et al., 2020; Liu et al., 2019). During the whole period, AAE was similar in spring and autumn indicating that light-absorbing aerosols were from similar emission sources in spring and autumn (Ran et al., 2016). AAE slightly increased in spring and autumn from 2018 to 2021. Part of the reason was the occurrence of multiple fugitive dust in spring and autumn (Yi et al., 2021; Gui et al., 2022). On the other hand, BrC could also be formed from secondary reactions (Bond et al., 2013; Wang et al., 2022). A slight increase in AAE in spring and autumn may also have been caused by a greater amount of secondary organic aerosol formation as a result of an increased atmospheric oxidation capacity (Ji et al., 2019; Lei et al., 2021).

The seasonal mean SSA increased in all seasons from 2018 to 2021, indicating that the contribution of scattering aerosols to extinction increased. This suggested that more effective control of scattering aerosols should be attached more importance in order to improve visibility in the future. In particular, SSA in winter increased significantly from 0.88 in 2018 to 0.93 in 2021, which revealed that the proportion of absorbing aerosols decreases considerably in winter. This is consistent with recent research which suggests that air pollution control measures has been more effective in reducing the primary pollution emissions than secondary species (Vu et al., 2019; Sun et al., 2020). On the other hand, seasonal mean SSA for PM_{10} was 0.94±0.04, 0.94±0.04, 0.92± 0.04, 0.93±0.03 in spring, summer, autumn, and winter 2021. Similar SSA suggests that the proportions of light absorbing and scattering components became relatively stable in four seasons.

Figure 3 shows the diurnal variations of σ_{ab} and SSA at 550 nm for PM_{10}, which are similar to those for PM_1 (Figure. S2). In the past four years, σ_{ab} was lower during the day and higher at night in four seasons. This was consistent with that observed at an urban site in Beijing during 2014-2016 (Wang et al., 2019). The evolution of the planetary boundary layer had an important influence on the diurnal variation of the σ_{ab}. With stronger solar radiation, the boundary layer was more fully developed during the daytime, and after sunset, the convective boundary layer underwent a transition to the nocturnal stable boundary layer (Guo et al., 2016). Furthermore, emissions also affected the diurnal variation of the σ_{ab}. For example, heavy-duty diesel trucks and heavy-duty vehicles were only allowed to enter urban areas from 23:00 to the following day 06:00 (Hu et al., 2021). As a response, the minimum σ_{ab} occurred during 12:00–18:00, when the planetary boundary layer was well-developed, and truck emission was lower. With shallow boundary layer height and enhanced emissions from heavy-duty trucks, σ_{ab} reached the maximum at night. During the study period, SSA showed a significant peak in the afternoon in four seasons, which was similar to previous studies in urban Beijing (Zhao et al., 2019; Wang et al., 2019). Higher SSA was shown in the afternoon, which was mainly related to the reduction of absorbing aerosols emission, and more secondary scattering aerosol produced by strong chemical reactions under intensive solar radiation and high temperature in the afternoon (Han et al., 2017).

3.2 Aerosol radiative effect

To study the climate impact of the aerosol particles, we investigated the variation of aerosol radiative forcing efficiency (RFE) at the top-of-the-atmosphere (TOA) variations.

As seen in Fig. 4, RFE for PM_{10} and PM_1 were always negative during the whole observation period, suggesting that the aerosols measured in urban Beijing have a stable cooling effect on the climate. RFE for PM_{10} and PM_1 at dry condition were −27.0 and -26.2 W m^{-2} AOD^{-1} in 2021 in urban Beijing, which was slightly negative than that of −24.9 W m^{-2} AOD^{-1} in Nanjing (Shen et al., 2018) and highly negative than that of −19.9 W m^{-2} AOD^{-1} in Finland (Virkkula et al., 2011). This suggested that the aerosols in urban Beijing have a higher cooling efficiency. In eq. (6) The fractional day length (D), solar constant (So), atmospheric transmission (T_{at}), fractional cloud amount (Ac), and surface reflectance (Rs) were constants, which were widely used in previous studies (Delene and Ogren, 2002; Andrews et al., 2011; Sherman et al., 2015; Shen et al., 2018). These values are the globally averaged values and don't always represent the conditions in Beijing, but using the same constants makes it possible to compare the intrinsic forcing efficiency of the aerosols measured at different stations around the world and to study how the RFE changes with varying SSA and b (Sherman et al., 2015; Luoma et al., 2019). On the other hand, RFE is sensitive to RH as the aerosol optical properties are different due to hygroscopic growth (Fierz-Schmidhauser et al., 2010; Luoma et al., 2019). Previous studies demonstrate that SSA increases with RH, while b decreases with increasing RH (Carrico et al., 2003; Cheng et al., 2008). The change of SSA to increase with RH and of b to decrease with RH will have opposite effects on the RFE, and thus to some extent, the RH dependencies of these two parameters will counterbalance each other (Luoma et al., 2019). Titos et al. (2021) found that the range of forcing enhancement in different types of sites varies from almost no enhancement up to a factor of 3–4 at RH=90 %. The results observed in urban Beijing showed that the aerosol radiative forcing at RH = 80 % was 1.48 times that under dry

conditions (Xia et al., 2023). RFE was calculated at a dry state in this study, while the atmosphere is not generally dry in the ambient air. Thus, the RFE in this study does not represent ambient conditions. The simplified RFE in this study does not represent the actual value for the aerosol forcing; however, it can still indicate how the changes in aerosol optical properties affect the climate (Delene and Ogren, 2002; Andrews et al., 2011; Sherman et al., 2015). RFE was affected by SSA and backscatter fraction (b) and we investigated the RFE variations with SSA and b in Beijing. As shown in Fig. 5, When SSA increases from 0.7 to 0.92, the mean RFE increases by 1.59 times, suggesting that SSA plays an important role in strengthening cooling efficiency. When SSA>0.92, the mean RFE relatively keeps constant. The approximate constant RFE does not mean that the absolute aerosol radiative forcing is constant; it just suggests that the intrinsic nature of the aerosol will not significantly affect the calculation of RFE (Andrews et al., 2011). Also, the backscatter fraction has a negative relationship with RFE. A lower values of backscatter fraction corresponds to larger particles (Luoma et al., 2019). RFE became more negative with increasing b, suggesting that smaller particles would cool the atmosphere more efficiently. During the study period, SSA increased from 0.89 to 0.93, while the yearly mean value of b was 0.13 every year during the study period. RFE became more negative from 2018 to 2021, suggesting that the efficiency of the aerosol cooling atmosphere was higher, which was mainly influenced by increasing SSA.

The ratio of ΔF/AOD is known as the aerosol radiative forcing efficiency (RFE) and ΔF at TOA was caculated by multiplying the RFE for PM_{10} with the AOD of ambient atmospheric aerosols observed at the CAMS site during the study periods. The mean value of ΔF from 2018-2021 was -15.0 W m^{-2}, -12.5 W m^{-2}, -12.1 W m^{-2}, and -11.8 W m^{-2},

respectively. Although RFE became more negative, the annual mean ΔF in 2021 corresponding to lower columnar aerosol loading became less negative than that of 2018 corresponding to higher columnar aerosol loading (Fig. S3) which was consistent with the analysis that aerosol loading was a essential factor for the estimation of ΔF (Andrews et al., 2011; Delene and Ogren, 2002).

3.3 Transport and its impact on aerosol optical properties in Beijing

In addition to local emissions, regional transport is also an important source of particulate matter in Beijing (Chang et al., 2019). Based on previous studies, aerosol source regions and air mass pathways could also affect aerosol optical properties, and the different origins of air masses showed different aerosol optical properties (Zhuang et al., 2015; Pu et al., 2015). The air mass back-trajectories analysis in the North China Plain revealed that the absorption coefficients and SSA were high when the air masses came from densely populated and highly industrial areas (Yan et al., 2008). Therefore, air mass back-trajectories were analyzed in this study to explore the regional transports' influence on aerosol optical properties. First, the air mass back trajectories during 2018–2021 were calculated and clustered (Fig. 7); then, we statistic the aerosol optical properties of each cluster from 2018-2021 (Fig. 8). Based on the Euclidean distance, the back trajectories were classified into five clusters, in which clusters 1, 2 and 3, which originated from the clean areas in Mongolia and eastern Inner Mongolia, and transported to Beijing along the pathway with low emissions, were corresponded to low σ_{ab} and low $PM_{2.5}$ (Fig. 8a, d). Cluster 4 from the south of Beijing and cluster 5 from the west of Beijing were referred to as the polluted air masses, and the average $PM_{2.5}$ concentrations and σ_{ab} of clusters 4 and

5 were higher than those of clusters 1, 2, and 3 in each year (Fig. 8a, d). Cluster 4 passed through Shandong and Hebei Province, which was heavily polluted before arriving in Beijing. Cluster 5 passed through polluted Shanxi and Hebei during transport. Higher σ_{ab} and $PM_{2.5}$ mass concentrations were mainly distributed in clusters 4 and 5 each year. Lower AAE in cluster 4 indicates that the southern air mass carries more freshly emitted BC particles. SSA of cluster 4 from the south was higher (Fig. 8b), which may relate to low $BC/PM_{2.5}$ ratios in south air masses (Xia et al., 2020). Zhang et al. (2013) found that high levels of secondary inorganic aerosols related to high humidity were transported by southern air masses, which enhanced heterogeneous reaction and leaded to relatively low $BC/PM_{2.5}$ ratios. Fig. 7b showed percentage of each cluster accounting for the total back trajectories in each year. The results indicated that variation in each cluster fraction from 2018 to 2021 was slight. In general, cluster 1-5 accounted for 19%-21%, 13%-17%, 16%-20%, 29%-36%, 12%-20% of total back trajectories, respectively. Notably, the percentage of polluted-relevant air masses (cluster 4 and cluster 5) was ~50% each year, indicating that the transport from the south and the west of has a considerable impact on the aerosol optical properties. σ_{ab} corresponding to clusters 4 and 5 decreased by 47.3% and 58.4%, and a decrease of $PM_{2.5}$ mass concentration from clusters 4 and 5 was 38.9% and 37.4% during 2018 - 2021 (Fig. 8a, d), which may result from the air quality has improved caused by control of source emissions in surrounding regions of Beijing. Therefore, the comprehensive control of atmospheric pollution in Beijing and surrounding regions would be highly effective in reducing air pollution in Beijing.

4 Conclusions

In this study, 4-year measurements of aerosol absorption properties and single scattering albedo for PM_{10} and PM_1 in Beijing were analyzed. The annual mean $PM_{2.5}$ in 2018 was 54.7 μg m^{-3}, and it decreased by 34.4% (35.9 μg m^{-3}) in 2021, which suggested that the strict pollution control measures are effective in reducing the PM loadings in Beijing. The annual mean σ_{ab} of PM_{10} and PM_1 decreased by 55.0% and 53.5%, respectively, and it showed a similar decrease in all seasons. Significant reduction in σ_{ab} may be related to reduced primary emissions caused by effective air pollution control measures. SSA at 550 nm increased from 0.89 ± 0.04 for PM_{10} (0.87 ± 0.05 for PM_1) in 2018 to 0.93 ± 0.03 for PM_{10} (0.91 ± 0.04 for PM_1) in 2021 and the seasonal averages of SSA for two sizes also increased in four seasons. Increasing SSA and decreasing $PM_{2.5}$ mass concentration suggest that the fraction of absorbing aerosols decreased with improved air quality due to pollution control measure-taking. During the study period, the annual average of Rab increased year by year and was up to 89.2% in 2021**,** indicating that fine particles are the main contributors to the total PM_{10} particle absorption, and the contributions from fine particles to absorption became more important in Beijing.

During the study period, AAE was lowest in summer and highest in winter. Seasonal mean AAE in summer was generally close to 1 indicating that freshly emitted BC from traffic sources was a major component of light-absorbing aerosols. The highest AAE highlights the importance of BrC light absorption in winter. Notably, AAE in winter decreased from 2018 to 2021, implying a decreasing contribution from BrC to absorption, which may relate to the effective control of biomass burning and coal combustion caused

by changes in heating energy structure. AAE in spring and autumn was similar, indicating light-absorbing aerosols were from similar emission sources in these two seasons.

Using a simple analytical equation, we investigated the aerosol radiative effect. Aerosol radiative forcing efficiency (RFE) for PM_{10} and PM_1 was always negative, suggesting that the aerosols measured in urban Beijing have a stable cooling effect on the climate. RFE for PM_{10} and PM_1 at dry conditions were −27.0 and -26.2 W m^{-2} AOD^{-1} in 2021 in urban Beijing. RFE was influenced by SSA and b. Higher b corresponds to more negative RFE suggesting that smaller particles larger would cool the atmosphere more efficiently. When SSA<0.92, the absolute value of mean RFE increased by 1.59 times, suggesting that SSA plays an important role in strengthening cooling efficiency. When SSA>0.92, the mean RFE keeps relatively constant, suggesting that the intrinsic nature of the aerosol will not significantly affect the calculation of RFE. SSA increased from 0.89 to 0.93, while the yearly mean value of b was 0.13 every year during the study period. RFE became more negative from 2018 to 2021, suggesting that the efficiency of the aerosol cooling atmosphere was higher, which was mainly influenced by increasing SSA.

Regional transport and its impact on aerosol optical properties were also analyzed. The air mass back trajectories arriving at Beijing were divided into five clusters. Clusters 1, 2, and 3, which originated from the clean area in Mongolia and eastern Inner Mongolia, were transported to Beijing along the pathway with low emissions, corresponding to low σ_{ab} and low $PM_{2.5}$. Air masses from south and west (Cluster 4 and Cluster 5), which both crossed the polluted region, always brought high $PM_{2.5}$ concentrations and σ_{ab}. σ_{ab} corresponding to clusters 4 and 5 decreased by 47.3% and 58.4%, and a decrease of $PM_{2.5}$ mass concentration from clusters 4 and 5 was 38.9% and 37.4% during 2018 - 2021, which

may result from the control of source emissions in surrounding regions of Beijing. Therefore, comprehensive control of atmospheric pollution in surrounding regions of Beijing is conducive to reducing pollution in Beijing.

Data availability.

The data in this study are available at: https://doi.org/10.5281/zenodo.7466069 (Hu et al., 2022)

Competing interests.

The authors declare that they have no conflict of interest.

Author contributions.

XH performed data analysis, prepared the figures and wrote the manuscript. JS designed the experiment and outlined the manuscript. XH, CX, and JS conducted the measurements. XS, YZ, QL, ZL, SZ, JW, AY, JL, SL and XZ discussed the results and commented on the manuscript.

Acknowledgments.

This study was supported by the National Natural Science Foundation of China (42090031, 41875147, 42075082, 42175128), Chinese Academy of Meteorological Sciences (2022KJ002, 2022KJ005, 2020KJ001, 2020Z002). It was also supported by the Innovation Team for Haze-fog Observation and Forecasts of MOST.

References

Anderson, T. L., and Ogren, J. A.: Determining Aerosol Radiative Properties Using the TSI 3563 Integrating Nephelometer, Aerosol Sci. Technol. , 29, 57-69, 10.1080/02786829808965551, 1998.

Andrews, E., Ogren, J. A., Bonasoni, P., Marinoni, A., Cuevas, E., Rodríguez, S., Sun, J. Y., Jaffe, D. A., Fischer, E. V., Baltensperger, U., Weingartner, E., Coen, M. C., Sharma, S., Macdonald, A. M., Leaitch, W. R., Lin, N. H., Laj, P., Arsov, T., Kalapov, I., Jefferson, A., and Sheridan, P.: Climatology of aerosol radiative properties in the free troposphere, Atmos. Res., 102, 365-393, 10.1016/j.atmosres.2011.08.017, 2011.

Bergin, M. H., Cass, G. R., Xu, J., Fang, C., Zeng, L. M., Yu, T., Salmon, L. G., Kiang, C. S., Tang, X. Y., Zhang, Y. H., and Chameides, W. L.: Aerosol radiative, physical, and chemical properties in Beijing during June 1999, J. Geophys. Res., 106, 17969-17980, 10.1029/2001jd900073, 2001.

Bond, T. C., Anderson, T. L., and Campbell, D.: Calibration and Intercomparison of Filter-Based Measurements of Visible Light Absorption by Aerosols, Aerosol Sci. Technol., 30, 582-600, 10.1080/027868299304435, 1999.

Bond, T. C., and Bergstrom, R. W.: Light Absorption by Carbonaceous Particles: An Investigative Review, Aerosol Sci. Technol., 40, 27-67, 10.1080/02786820500421521, 2007.

Bond, T. C., Doherty, S. J., Fahey, D. W., Forster, P. M., Berntsen, T., DeAngelo, B. J., Flanner, M. G., Ghan, S., Kärcher, B., Koch, D., Kinne, S., Kondo, Y., Quinn, P. K., Sarofim, M. C., Schultz, M. G., Schulz, M., Venkataraman, C., Zhang, H., Zhang, S., Bellouin, N., Guttikunda, S. K., Hopke, P. K., Jacobson, M. Z., Kaiser, J. W., Klimont, Z., Lohmann, U.,

529 Schwarz, J. P., Shindell, D., Storelvmo, T., Warren, S. G., and Zender, C. S.: Bounding the
530 role of black carbon in the climate system: A scientific assessment, J. Geophys. Res.-
531 Atmos., 118, 5380-5552, 10.1002/jgrd.50171, 2013.
532 Carrico, C. M., Rood, P. K. a. M. J., and Bates, P. K. Q. a. T. S.: Mixtures of pollution, dust,
533 sea salt, and volcanic aerosol during ACE-Asia: Radiative properties as a function of
534 relative humidity, J. Geophys. Res., 108, 8650, 10.1029/2003jd003405, 2003.
535 Chang, X., Wang, S., Zhao, B., Xing, J., Liu, X., Wei, L., Song, Y., Wu, W., Cai, S., Zheng,
536 H., Ding, D., and Zheng, M.: Contributions of inter-city and regional transport to PM2.5
537 concentrations in the Beijing-Tianjin-Hebei region and its implications on regional joint air
538 pollution control, Sci Total Environ, 660, 1191-1200, 10.1016/j.scitotenv.2018.12.474,
539 2019.
540 Charlson, R. J., Schwartz, S. E., Hales, J. M., Cess, R. D., Coakley, J. A., Hansen, J. E.,
541 and Hofmann, D. J.: Climate Forcing by Anthropogenic Aerosols, Science, 255, 423-430,
542 10.1126/science.255.5043.423, 1992.
543 Cheng, Y. F., Wiedensohler, A., Eichler, H., Su, H., Gnauk, T., Brüggemann, E., Herrmann,
544 H., Heintzenberg, J., Slanina, J., and Tuch, T.: Aerosol optical properties and related
545 chemical apportionment at Xinken in Pearl River Delta of China, Atmospheric
546 Environment, 42, 6351-6372, 10.1016/j.atmosenv.2008.02.034, 2008.
547 Collaud Coen, M., Andrews, E., Asmi, A., Baltensperger, U., Bukowiecki, N., Day, D.,
548 Fiebig, M., Fjaeraa, A. M., Flentje, H., Hyvärinen, A., Jefferson, A., Jennings, S. G.,
549 Kouvarakis, G., Lihavainen, H., Lund Myhre, C., Malm, W. C., Mihapopoulos, N., Molenar,
550 J. V., amp, apos, Dowd, C., Ogren, J. A., Schichtel, B. A., Sheridan, P., Virkkula, A.,
551 Weingartner, E., Weller, R., and Laj, P.: Aerosol decadal trends – Part 1: In-situ optical

552 measurements at GAW and IMPROVE stations, Atmos. Chem. Phys., 13, 869-894,
553 10.5194/acp-13-869-2013, 2013.
554 Collaud Coen, M., Andrews, E., Alastuey, A., Arsov, T. P., Backman, J., Brem, B. T.,
555 Bukowiecki, N., Couret, C., Eleftheriadis, K., Flentje, H., Fiebig, M., Gysel-Beer, M.,
556 Hand, J. L., Hoffer, A., Hooda, R., Hueglin, C., Joubert, W., Keywood, M., Kim, J. E., Kim,
557 S.-W., Labuschagne, C., Lin, N.-H., Lin, Y., Lund Myhre, C., Luoma, K., Lyamani, H.,
558 Marinoni, A., Mayol-Bracero, O. L., Mihalopoulos, N., Pandolfi, M., Prats, N., Prenni, A.
559 J., Putaud, J.-P., Ries, L., Reisen, F., Sellegri, K., Sharma, S., Sheridan, P., Sherman, J. P.,
560 Sun, J., Titos, G., Torres, E., Tuch, T., Weller, R., Wiedensohler, A., Zieger, P., and Laj, P.:
561 Multidecadal trend analysis of in situ aerosol radiative properties around the world,
562 Atmospheric Chemistry and Physics, 20, 8867-8908, 10.5194/acp-20-8867-2020, 2020.
563 Dai, M., Zhu, B., Fang, C., Zhou, S., Lu, W., Zhao, D., Ding, D., Pan, C., and Liao, H.:
564 Long-Term Variation and Source Apportionment of Black Carbon at Mt. Waliguan, China,
565 Journal of Geophysical Research: Atmospheres, 126, 10.1029/2021jd035273, 2021.
566 Davies, N. W., Fox, C., Szpek, K., Cotterell, M. I., Taylor, J. W., Allan, J. D., Williams, P.
567 I., Trembath, J., Haywood, J. M., and Langridge, J. M.: Evaluating biases in filter-based
568 aerosol absorption measurements using photoacoustic spectroscopy, Atmos. Meas. Tech.,
569 12, 3417-3434, 10.5194/amt-12-3417-2019, 2019.
570 Delene, D. J., and Ogren, J. A.: Variability of Aerosol Optical Properties at Four North
571 American Surface Monitoring Sites, J. Aerosol Sci., 59, 1135-1150, 10.1175/1520-
572 0469(2002)059<1135:VOAOPA>2.0.CO;2, 2002.
573 Draxler, R. R., and Hess, G. D.: An overview of the HYSPLIT_4 modelling system of
574 trajectories, dispersion, and deposition, Aust. Meteor. Mag., 47, 295-308, 1998.

575 Dumka, U. C., Kaskaoutis, D. G., Srivastava, M. K., and Devara, P. C. S.: Scattering and
576 absorption properties of near-surface aerosol over Gangetic–Himalayan region: the role of
577 boundary-layer dynamics and long-range transport, Atmospheric Chemistry and Physics,
578 15, 1555-1572, 10.5194/acp-15-1555-2015, 2015.
579 Ealo, M., Alastuey, A., Pérez, N., Ripoll, A., Querol, X., and Pandolfi, M.: Impact of
580 aerosol particle sources on optical properties in urban, regional and remote areas in the
581 north-western Mediterranean, Atmos. Chem. Phys., 18, 1149-1169, 10.5194/acp-18-1149-
582 2018, 2018.
583 Fierz-Schmidhauser, R., Zieger, P., Gysel, M., Kammermann, L., DeCarlo, P. F.,
584 Baltensperger, U., and Weingartner, E.: Measured and predicted aerosol light scattering
585 enhancement factors at the high alpine site Jungfraujoch, Atmos. Chem. Phys., 10, 2319–
586 2333, 2010.
587 Garland, R. M., Schmid, O., Nowak, A., Achtert, P., Wiedensohler, A., Gunthe, S. S.,
588 Takegawa, N., Kita, K., Kondo, Y., and Hu, M.: Aerosol optical properties observed during
589 Campaign of Air Quality Research in Beijing 2006 (CAREBeijing-2006): Characteristic
590 differences between the inflow and outflow of Beijing city air, J. Geophys. Res., 114,
591 D00G04, 10.1029/2008JD010780, 2009.
592 Gong, S., Zhang, L., Liu, C., Lu, S., Pan, W., and Zhang, Y.: Multi-scale analysis of the
593 impacts of meteorology and emissions on PM(2.5) and O(3) trends at various regions in
594 China from 2013 to 2020 2. Key weather elements and emissions, Sci Total Environ, 824,
595 153847, 10.1016/j.scitotenv.2022.153847, 2022.
596 Gui, K., Yao, W., Che, H., An, L., Zheng, Y., Li, L., Zhao, H., Zhang, L., Zhong, J., Wang,
597 Y., and Zhang, X.: Record-breaking dust loading during two mega dust storm events over

598 northern China in March 2021: aerosol optical and radiative properties and meteorological
599 drivers, Atmos. Chem. Phys., 22, 7905-7932, 10.5194/acp-22-7905-2022, 2022.
600 Guo, J., Miao, Y., Zhang, Y., Liu, H., Li, Z., Zhang, W., He, J., Lou, M., Yan, Y., Bian, L.,
601 and Zhai, P.: The climatology of planetary boundary layer height in China derived from
602 radiosonde and reanalysis data, Atmos. Chem. Phys., 16, 13309-13319, 10.5194/acp-16-
603 13309-2016, 2016.
604 Han, T., Xu, W., Li, J., Freedman, A., Zhao, J., Wang, Q., Chen, C., Zhang, Y., Wang, Z.,
605 Fu, P., Liu, X., and Sun, Y.: Aerosol optical properties measurements by a CAPS single
606 scattering albedo monitor: Comparisons between summer and winter in Beijing, China, J.
607 Geophys. Res.-Atmos., 122, 2513-2526, 10.1002/2016jd025762, 2017.
608 Haywood, J. M., and Shine, K. P.: The effect of anthropogenic sulfate and soot aerosol on
609 the clear sky planetary radiation budget, Geophys. Res. Lett., 22(5), 603-606,
610 10.1029/95GL00075, 1995.
611 He, X., Li, C. C., Lau, A. K. H., Deng, Z. Z., Mao, J. T., Wang, M., and Liu, X., Y.: An
612 intensive study of aerosol optical properties in Beijing urban area, Atmos. Chem. Phys., 9,
613 8903-8915, 10.5194/acp-9-8903-2009, 2009.
614 Helin, A., Virkkula, A., Backman, J., Pirjola, L., Sippula, O., Aakko-Saksa, P., Väätäinen,
615 S., Mylläri, F., Järvinen, A., Bloss, M., Aurela, M., Jakobi, G., Karjalainen, P.,
616 Zimmermann, R., Jokiniemi, J., Saarikoski, S., Tissari, J., Rönkkö, T., Niemi, J. V., and
617 Timonen, H.: Variation of Absorption Ångström Exponent in Aerosols From Different
618 Emission Sources, J. Geophys. Res.-Atmos., 126, 10.1029/2020jd034094, 2021.
619 Hu, X., Sun, J., Xia, C., Shen, X., Zhang, Y., Zhang, X., and Zhang, S.: Simultaneous
620 measurements of PM1 and PM10 aerosol scattering properties and their relationships in

621 urban Beijing: A two-year observation, Sci. Total Environ., 770, 145215,
622 10.1016/j.scitotenv.2021.145215, 2021.
623 Hu, X., Sun, J., Xia, C., Shen, X., Zhang, Y., Liu, Q., Liu, Z., Zhang, S., Wang, J., Yu, A.,
624 Lu, J., Liu, S., and Zhang, X.: Rapid decline of aerosol absorption coefficient and aerosol
625 optical properties effects on radiative forcing in urban areas of Beijing from 2018 to 2021
626 [Data set], Zenodo, https://doi.org/10.5281/zenodo.7466069, 2022.
627 J. Hansen, M. Sato, and Ruedy, R.: Radiative forcing and climate response, J. Geophys.
628 Res., 102, 6831-6864, 10.1029/96jd03436, 1997.
629 Jacobson, M. Z.: Strong radiative heating due to the mixing state of black carbon in
630 atmospheric aerosols, Nature, 409, 695-697, 10.1038/35055518, 2001.
631 Ji, D., Gao, W., Maenhaut, W., He, J., Wang, Z., Li, J., Du, W., Wang, L., Sun, Y., Xin, J.,
632 Hu, B., and Wang, Y.: Impact of air pollution control measures and regional transport on
633 carbonaceous aerosols in fine particulate matter in urban Beijing, China: insights gained
634 from long-term measurement, Atmos. Chem. Phys., 19, 8569-8590, 10.5194/acp-19-8569-
635 2019, 2019.
636 Ji, D., Li, J., Shen, G., He, J., Gao, W., Tao, J., Liu, Y., Tang, G., Zeng, L., Zhang, R., and
637 Wang, Y.: Environmental effects of China's coal ban policy: Results from in situ
638 observations and model analysis in a typical rural area of the Beijing-Tianjin-Hebei region,
639 China, Atmos. Res., 268, 10.1016/j.atmosres.2022.106015, 2022.
640 Jia, M., Evangeliou, N., Eckhardt, S., Huang, X., Gao, J., Ding, A., and Stohl, A.: Black
641 Carbon Emission Reduction Due to COVID-19 Lockdown in China, Geophys Res Lett, 48,
642 e2021GL093243, 10.1029/2021GL093243, 2021.
643 Jing, J., Wu, Y., Tao, J., Che, H., Xia, X., Zhang, X., Yan, P., Zhao, D., and Zhang, L.:

644 Observation and analysis of near-surface atmospheric aerosol optical properties in urban
645 Beijing, Particuology, 18, 144-154, 10.1016/j.partic.2014.03.013, 2015.
646 Lack, D. A., and Cappa, C. D.: Impact of brown and clear carbon on light absorption
647 enhancement, single scatter albedo and absorption wavelength dependence of black carbon,
648 Atmos. Chem. Phys., 10, 4207-4220, 10.5194/acp-10-4207-2010, 2010.
649 Laj, P., Bigi, A., Rose, C., Andrews, E., Lund Myhre, C., Collaud Coen, M., Lin, Y.,
650 Wiedensohler, A., Schulz, M., Ogren, J. A., Fiebig, M., Gliß, J., Mortier, A., Pandolfi, M.,
651 Petäja, T., Kim, S.-W., Aas, W., Putaud, J.-P., Mayol-Bracero, O., Keywood, M., Labrador,
652 L., Aalto, P., Ahlberg, E., Alados Arboledas, L., Alastuey, A., Andrade, M., Artíñano, B.,
653 Ausmeel, S., Arsov, T., Asmi, E., Backman, J., Baltensperger, U., Bastian, S., Bath, O.,
654 Beukes, J. P., Brem, B. T., Bukowiecki, N., Conil, S., Couret, C., Day, D., Dayantolis, W.,
655 Degorska, A., Eleftheriadis, K., Fetfatzis, P., Favez, O., Flentje, H., Gini, M. I., Gregorič,
656 A., Gysel-Beer, M., Hallar, A. G., Hand, J., Hoffer, A., Hueglin, C., Hooda, R. K.,
657 Hyvärinen, A., Kalapov, I., Kalivitis, N., Kasper-Giebl, A., Kim, J. E., Kouvarakis, G.,
658 Kranjc, I., Krejci, R., Kulmala, M., Labuschagne, C., Lee, H.-J., Lihavainen, H., Lin, N.-
659 H., Löschau, G., Luoma, K., Marinoni, A., Martins Dos Santos, S., Meinhardt, F., Merkel,
660 M., Metzger, J.-M., Mihalopoulos, N., Nguyen, N. A., Ondracek, J., Pérez, N., Perrone, M.
661 R., Petit, J.-E., Picard, D., Pichon, J.-M., Pont, V., Prats, N., Prenni, A., Reisen, F., Romano,
662 S., Sellegri, K., Sharma, S., Schauer, G., Sheridan, P., Sherman, J. P., Schütze, M., Schwerin,
663 A., Sohmer, R., Sorribas, M., Steinbacher, M., Sun, J., Titos, G., Toczko, B., Tuch, T., Tulet,
664 P., Tunved, P., Vakkari, V., Velarde, F., Velasquez, P., Villani, P., Vratolis, S., Wang, S.-H.,
665 Weinhold, K., Weller, R., Yela, M., Yus-Diez, J., Zdimal, V., Zieger, P., and Zikova, N.: A
666 global analysis of climate-relevant aerosol properties retrieved from the network of Global

667 Atmosphere Watch (GAW) near-surface observatories, Atmospheric Measurement
668 Techniques, 13, 4353-4392, 10.5194/amt-13-4353-2020, 2020.
669 Le, T., Wang, Y., Liu, L., Yang, J., Yung, Y. L., Li, G., and Seinfeld, J. H.: Unexpected air
670 pollution with marked emission reductions during the COVID-19 outbreak in China,
671 Science, 369, 702-706, 10.1126/science.abb7431, 2020.
672 Lee, K. H., Li, Z., Wong, M. S., Xin, J., Wang, Y., Hao, W.-M., and Zhao, F.: Aerosol single
673 scattering albedo estimated across China from a combination of ground and satellite
674 measurements, J. Geophys. Res., 112, 10.1029/2007jd009077, 2007.
675 Lei, L., Zhou, W., Chen, C., He, Y., Li, Z., Sun, J., Tang, X., Fu, P., Wang, Z., and Sun, Y.:
676 Long-term characterization of aerosol chemistry in cold season from 2013 to 2020 in
677 Beijing, China, Environ. Pollut., 268, 115952, 10.1016/j.envpol.2020.115952, 2021.
678 Li, J., Carlson, B. E., Yung, Y. L., Lv, D., Hansen, J., Penner, J. E., Liao, H., Ramaswamy,
679 V., Kahn, R. A., Zhang, P., Dubovik, O., Ding, A., Lacis, A. A., Zhang, L., and Dong, Y.:
680 Scattering and absorbing aerosols in the climate system, Nature Reviews Earth &
681 Environment, 10.1038/s43017-022-00296-7, 2022a.
682 Li, W., Liu, X., Duan, F., Qu, Y., and An, J.: A one-year study on black carbon in urban
683 Beijing: Concentrations, sources and implications on visibility, Atmos. Pollut. Res., 13,
684 10.1016/j.apr.2021.101307, 2022b.
685 Liu, G. J., Xin, J. Y., Wang, X., Si, R. R., Ma, Y. N., Wen, T. X., Zhao, L., Zhao, D. D.,
686 Wang, Y. S., and Gao, W. K.: Impact of the coal banning zone on visibility in the Beijing-
687 Tianjin-Hebei region, Sci. Total Environ., 692, 402-410, 10.1016/j.scitotenv.2019.07.006,
688 2019.
689 Liu, Y., Wang, Y., Cao, Y., Yang, X., Zhang, T., Luan, M., Lyu, D., Hansen, A. D. A., Liu,

690 B., and Zheng, M.: Impacts of COVID-19 on Black Carbon in Two Representative Regions
691 in China: Insights Based on Online Measurement in Beijing and Tibet, Geophysical
692 Research Letters, 48, 10.1029/2021gl092770, 2021.
693 Luo, L., Tian, H., Liu, H., Bai, X., Liu, W., Liu, S., Wu, B., Lin, S., Zhao, S., Hao, Y., Sun,
694 Y., Hao, J., and Zhang, K.: Seasonal variations in the mass characteristics and optical
695 properties of carbonaceous constituents of PM2.5 in six cities of North China, Environ.
696 Pollut., 268, 115780, 10.1016/j.envpol.2020.115780, 2020.
697 Luoma, K., Virkkula, A., Aalto, P., Petäjä, T., and Kulmala, M.: Over a 10-year record of
698 aerosol optical properties at SMEAR II, Atmos. Chem. Phys., 19, 11363-11382,
699 10.5194/acp-19-11363-2019, 2019.
700 Moosmüller, H., Chakrabarty, R. K., and Arnott, W. P.: Aerosol light absorption and its
701 measurement: A review, J. Quant. Spectrosc. Radiat. Transf., 110, 844-878,
702 10.1016/j.jqsrt.2009.02.035, 2009.
703 Ogren, J. A., Wendell, J., Andrews, E., and Sheridan, P. J.: Continuous light absorption
704 photometer for long-term studies, Atmos. Meas. Tech., 10, 4805-4818, 10.5194/amt-10-
705 4805-2017, 2017.
706 Pandolfi, M., Alados-Arboledas, L., Alastuey, A., Andrade, M., Angelov, C., Artiñano, B.,
707 Backman, J., Baltensperger, U., Bonasoni, P., Bukowiecki, N., Collaud Coen, M., Conil,
708 S., Coz, E., Crenn, V., Dudoitis, V., Ealo, M., Eleftheriadis, K., Favez, O., Fetfatzis, P.,
709 Fiebig, M., Flentje, H., Ginot, P., Gysel, M., Henzing, B., Hoffer, A., Holubova Smejkalova,
710 A., Kalapov, I., Kalivitis, N., Kouvarakis, G., Kristensson, A., Kulmala, M., Lihavainen,
711 H., Lunder, C., Luoma, K., Lyamani, H., Marinoni, A., Mihalopoulos, N., Moerman, M.,
712 Nicolas, J., amp, apos, Dowd, C., Petäjä, T., Petit, J.-E., Pichon, J. M., Prokopciuk, N.,

713 Putaud, J.-P., Rodríguez, S., Sciare, J., Sellegri, K., Swietlicki, E., Titos, G., Tuch, T.,
714 Tunved, P., Ulevicius, V., Vaishya, A., Vana, M., Virkkula, A., Vratolis, S., Weingartner, E.,
715 Wiedensohler, A., and Laj, P.: A European aerosol phenomenology – 6: scattering
716 properties of atmospheric aerosol particles from 28 ACTRIS sites, Atmospheric Chemistry
717 and Physics, 18, 7877-7911, 10.5194/acp-18-7877-2018, 2018.
718 Pu, W., Zhao, X., Shi, X., Ma, Z., Zhang, X., and Yu, B.: Impact of long-range transport on
719 aerosol properties at a regional background station in Northern China, Atmospheric
720 Research, 153, 489-499, 10.1016/j.atmosres.2014.10.010, 2015.
721 Ran, L., Deng, Z. Z., Wang, P. C., and Xia, X. A.: Black carbon and wavelength-dependent
722 aerosol absorption in the North China Plain based on two-year aethalometer measurements,
723 Atmos. Environ., 142, 132-144, 10.1016/j.atmosenv.2016.07.014, 2016.
724 Segura, S., Estellés, V., Esteve, A. R., Marcos, C. R., Utrillas, M. P., and Martínez-Lozano,
725 J. A.: Multiyear in-situ measurements of atmospheric aerosol absorption properties at an
726 urban coastal site in western Mediterranean, Atmos. Environ., 129, 18-26,
727 10.1016/j.atmosenv.2016.01.008, 2016.
728 Shen, Y., Virkkula, A., Ding, A., Wang, J., Chi, X., Nie, W., Qi, X., Huang, X., Liu, Q.,
729 Zheng, L., Xu, Z., Petäjä, T., Aalto, P. P., Fu, C., and Kulmala, M.: Aerosol optical
730 properties at SORPES in Nanjing, east China, Atmos. Chem. Phys., 18, 5265-5292,
731 10.5194/acp-18-5265-2018, 2018.
732 Sheridan, P. J., and Ogren, J. A.: Observations of the vertical and regional variability of
733 aerosol optical properties over central and eastern North America, J. Geophys. Res., 104,
734 16793-16805, 10.1029/1999jd900241, 1999.
735 Sherman, J. P., Sheridan, P. J., Ogren, J. A., Andrews, E., Hageman, D., Schmeisser, L.,

736 Jefferson, A., and Sharma, S.: A multi-year study of lower tropospheric aerosol variability
737 and systematic relationships from four North American regions, Atmospheric Chemistry
738 and Physics, 15, 12487-12517, 10.5194/acp-15-12487-2015, 2015.
739 Sun, J., Wang, Z., Zhou, W., Xie, C., Wu, C., Chen, C., Han, T., Wang, Q., Li, Z., Li, J., Fu,
740 P., Wang, Z., and Sun, Y.: Measurement report: Long-term changes in black carbon and
741 aerosol optical properties from 2012 to 2020 in Beijing, China, Atmos. Chem. Phys., 22,
742 561-575, 10.5194/acp-22-561-2022, 2022.
743 Sun, Y., Xu, W., Zhang, Q., Jiang, Q., Canonaco, F., Prévôt, A. S. H., Fu, P., Li, J., Jayne,
744 J., Worsnop, D. R., and Wang, Z.: Source apportionment of organic aerosol from 2-year
745 highly time-resolved measurements by an aerosol chemical speciation monitor in Beijing,
746 China, Atmos. Chem. Phys., 18, 8469-8489, 10.5194/acp-18-8469-2018, 2018.
747 Sun, Y., Lei, L., Zhou, W., Chen, C., He, Y., Sun, J., Li, Z., Xu, W., Wang, Q., Ji, D., Fu, P.,
748 Wang, Z., and Worsnop, D. R.: A chemical cocktail during the COVID-19 outbreak in
749 Beijing, China: Insights from six-year aerosol particle composition measurements during
750 the Chinese New Year holiday, Sci Total Environ, 742, 140739,
751 10.1016/j.scitotenv.2020.140739, 2020.
752 Szopa, S., Naik, V., Adhikary, B., Artaxo, P., Berntsen, T., Collins, W. D., Fuzzi, S.,
753 Gallardo, L., Kiendler-Scharr, A., Klimont, Z., Liao, H., Unger, N., and Zanis, P.: Short-
754 Lived Climate Forcers. In Climate Change 2021: The Physical Science Basis. Contribution
755 of Working Group I to the Sixth Assessment Report of the Intergovernmental Panel on
756 Climate Change [Masson-Delmotte, V., P. Zhai, A. Pirani, S.L. Connors, C. Péan, S. Berger,
757 N. Caud, Y. Chen, L. Goldfarb, M.I. Gomis, M. Huang, K. Leitzell, E. Lonnoy, J.B.R.
758 Matthews, T.K. Maycock, T. Waterfield, O. Yelekçi, R. Yu, and B. Zhou (eds.)], Cambridge

759 University Press, Cambridge, United Kingdom and New York, NY, USA, 817-922,
760 10.1017/9781009157896.008, 2021.
761 Tian, H., Liu, Y., Li, Y., Wu, C. H., Chen, B., Kraemer, M. U. G., Li, B., Cai, J., Xu, B.,
762 Yang, Q., Wang, B., Yang, P., Cui, Y., Song, Y., Zheng, P., Wang, Q., Bjornstad, O. N., Yang,
763 R., Grenfell, B. T., Pybus, O. G., and Dye, C.: An investigation of transmission control
764 measures during the first 50 days of the COVID-19 epidemic in China, Science, 368, 638-
765 642, 10.1126/science.abb6105, 2020.
766 Titos, G., Foyo-Moreno, I., Lyamani, H., Querol, X., Alastuey, A., and Alados-Arboledas,
767 L.: Optical properties and chemical composition of aerosol particles at an urban location:
768 An estimation of the aerosol mass scattering and absorption efficiencies, Journal of
769 Geophysical Research, 117, D04206, 10.1029/2011jd016671, 2012.
770 Titos, G., Burgos, M. A., Zieger, P., Alados-Arboledas, L., Baltensperger, U., Jefferson, A.,
771 Sherman, J., Weingartner, E., Henzing, B., Luoma, K., O'Dowd, C., Wiedensohler, A., and
772 Andrews, E.: A global study of hygroscopicity-driven light-scattering enhancement in the
773 context of other in situ aerosol optical properties, Atmospheric Chemistry and Physics, 21,
774 13031-13050, 10.5194/acp-21-13031-2021, 2021.
775 Tuch, T. M., Haudek, A., Müller, T., Nowak, A., Wex, H., and Wiedensohler, A.: Design
776 and performance of an automatic regenerating adsorption aerosol dryer for continuous
777 operation at monitoring sites, Atmos. Meas. Tech., 2, 417-422, 10.5194/amt-2-417-2009,
778 2009.
779 Twomey, S.: Pollution and the Planetary Albedo, Atmos. Environ., 41, 120-125,
780 10.1016/j.atmosenv.2007.10.062, 2007.
781 Virkkula, A., Backman, J., Aalto, P. P., Hulkkonen, M., Riuttanen, L., Nieminen, T., dal

782 Maso, M., Sogacheva, L., de Leeuw, G., and Kulmala, M.: Seasonal cycle, size
783 dependencies, and source analyses of aerosol optical properties at the SMEAR II
784 measurement station in Hyytiälä, Finland, Atmos. Chem. Phys., 11, 4445-4468,
785 10.5194/acp-11-4445-2011, 2011.
786 Vu, T. V., Shi, Z., Cheng, J., Zhang, Q., He, K., Wang, S., and Harrison, R. M.: Assessing
787 the impact of clean air action on air quality trends in Beijing using a machine learning
788 technique, Atmospheric Chemistry and Physics, 19, 11303-11314, 10.5194/acp-19-11303-
789 2019, 2019.
790 Wang, Q. L., Wang, L. L., Gong, C. S., Li, M. G., Xin, J. Y., Tang, G. Q., Sun, Y., Gao, J.
791 H., Wang, Y. H., Wu, S., Kang, Y. Y., Yang, Y., Li, T. T., Liu, J. D., and Wang, Y. S.: Vertical
792 evolution of black and brown carbon during pollution events over North China Plain, Sci.
793 Total Environ., 806, ARTN 150950
794 10.1016/j.scitotenv.2021.150950, 2022.
795 Wang, T., Du, Z., Tan, T., Xu, N., Hu, M., Hu, J., and Guo, S.: Measurement of aerosol
796 optical properties and their potential source origin in urban Beijing from 2013-2017, Atmos.
797 Environ., 206, 293-302, 10.1016/j.atmosenv.2019.02.049, 2019.
798 Wang, Y. Q., Zhang, X. Y., and Draxler, R. R.: TrajStat: GIS-based software that uses
799 various trajectory statistical analysis methods to identify potential sources from long-term
800 air pollution measurement data, Environ. Model Softw., 24, 938-939,
801 10.1016/j.envsoft.2009.01.004, 2009.
802 WMO/GAW: WMO/GAW Aerosol Measurement Procedures, Guidelines and
803 Recommendations, Geneva, Switzerland, 2016.
804 Xia, C., Sun, J., Qi, X., Shen, X., Zhong, J., Zhang, X., Wang, Y., Zhang, Y., and Hu, X.:

805 Observational study of aerosol hygroscopic growth on scattering coefficient in Beijing: A
806 case study in March of 2018, Sci. Total Environ., 685, 239-247,
807 10.1016/j.scitotenv.2019.05.283, 2019.
808 Xia, C., Sun, J., Hu, X., Shen, X., Zhang, Y., Zhang, S., Wang, J., Liu, Q., Lu, J., Liu, S.,
809 and Zhang, X.: Effects of hygroscopicity on aerosol optical properties and direct radiative
810 forcing in Beijing: Based on two-year observations, Sci Total Environ, 857, 159233,
811 10.1016/j.scitotenv.2022.159233, 2023.
812 Xia, Y., Wu, Y., Huang, R. J., Xia, X., Tang, J., Wang, M., Li, J., Wang, C., Zhou, C., and
813 Zhang, R.: Variation in black carbon concentration and aerosol optical properties in Beijing:
814 Role of emission control and meteorological transport variability, Chemosphere, 254,
815 126849, 10.1016/j.chemosphere.2020.126849, 2020.
816 Xie, C., He, Y., Lei, L., Zhou, W., Liu, J., Wang, Q., Xu, W., Qiu, Y., Zhao, J., Sun, J., Li,
817 L., Li, M., Zhou, Z., Fu, P., Wang, Z., and Sun, Y.: Contrasting mixing state of black carbon-
818 containing particles in summer and winter in Beijing, Environ. Pollut., 263, 114455,
819 10.1016/j.envpol.2020.114455, 2020.
820 Xu, X., and Zhang, T.: Spatial-temporal variability of PM2.5 air quality in Beijing, China
821 during 2013-2018, J. Environ. Manag., 262, 110263, 10.1016/j.jenvman.2020.110263,
822 2020.
823 Yan, P., Tang, J., Huang, J., Mao, J. T., Zhou, X. J., Liu, Q., Wang, Z. F., and Zhou, H. G.:
824 The measurement of aerosol optical properties at a rural site in Northern China,
825 Atmospheric Chemistry and Physics, 8, 2229–2242, 10.5194/acp-8-2229-2008, 2008.
826 Yang, M., Howell, S. G., Zhuang, J., and Huebert, B. J.: Attribution of aerosol light
827 absorption to black carbon, brown carbon, and dust in China – interpretations of

atmospheric measurements during EAST-AIRE, Atmos. Chem. Phys., 9, 2035–2050, 2009.

Yi, Z., Wang, Y., Chen, W., Guo, B., Zhang, B., Che, H., and Zhang, X.: Classification of the Circulation Patterns Related to Strong Dust Weather in China Using a Combination of the Lamb–Jenkinson and k-Means Clustering Methods, Atmosphere, 12, 10.3390/atmos12121545, 2021.

Zhang, Q., Zheng, Y., Tong, D., Shao, M., Wang, S., Zhang, Y., Xu, X., Wang, J., He, H., Liu, W., Ding, Y., Lei, Y., Li, J., Wang, Z., Zhang, X., Wang, Y., Cheng, J., Liu, Y., Shi, Q., Yan, L., Geng, G., Hong, C., Li, M., Liu, F., Zheng, B., Cao, J., Ding, A., Gao, J., Fu, Q., Huo, J., Liu, B., Liu, Z., Yang, F., He, K., and Hao, J.: Drivers of improved $PM_{2.5}$ air quality in China from 2013 to 2017, P. Natl. Acad. Sci. USA, 116, 24463-24469, 10.1073/pnas.1907956116, 2019.

Zhang, R., Jing, J., Tao, J., Hsu, S. C., Wang, G., Cao, J., Lee, C. S. L., Zhu, L., Chen, Z., Zhao, Y., and Shen, Z.: Chemical characterization and source apportionment of PM2.5 in Beijing: seasonal perspective, Atmos. Chem. Phys., 13, 7053-7074, 10.5194/acp-13-7053-2013, 2013.

Zhang, Y. Z., Zhi, G. R., Jin, W. J., Wang, L., Guo, S. C., Shi, R., Sun, J. Z., Cheng, M. M., Bi, F., Gao, J., Zhang, B. J., Wu, J. J., Shi, Z. H., Liu, B., Wang, Z., and Li, S. Y.: Differing effects of escalating pollution on absorption and scattering efficiencies of aerosols: Toward co-beneficial air quality enhancement and climate protection measures, Atmos. Environ., 232, 10.1016/j.atmosenv.2020.117570, 2020.

Zhao, S. M., Hu, B., Du, C. J., Tang, L. Q., Ma, Y. J., Liu, H., Zou, J. N., Liu, Z. R., Wei, J., and Wang, Y. S.: Aerosol optical characteristics and radiative forcing in urban Beijing, Atmos. Environ., 212, 41-53, 10.1016/j.atmosenv.2019.05.034, 2019.

Zhao, S. M., Hu, B., Gao, W. K., Li, L. C., Huang, W., Wang, L. L., Yang, Y., Liu, J. D., Li, J. Y., Ji, D. S., Zhang, R. J., Zhang, Y. Y., and Wang, Y. S.: Effect of the "coal to gas" project on atmospheric NOX during the heating period at a suburban site between Beijing and Tianjin, Atmos. Res., 241, 10.1016/j.atmosres.2020.104977, 2020.

Zhuang, B. L., Wang, T. J., Liu, J., Ma, Y., Yin, C. Q., Li, S., Xie, M., Han, Y., Zhu, J. L., Yang, X. Q., and Fu, C. B.: Absorption coefficient of urban aerosol in Nanjing, west Yangtze River Delta, China, Atmos. Chem. Phys., 15, 13633-13646, 10.5194/acp-15-13633-2015, 2015.

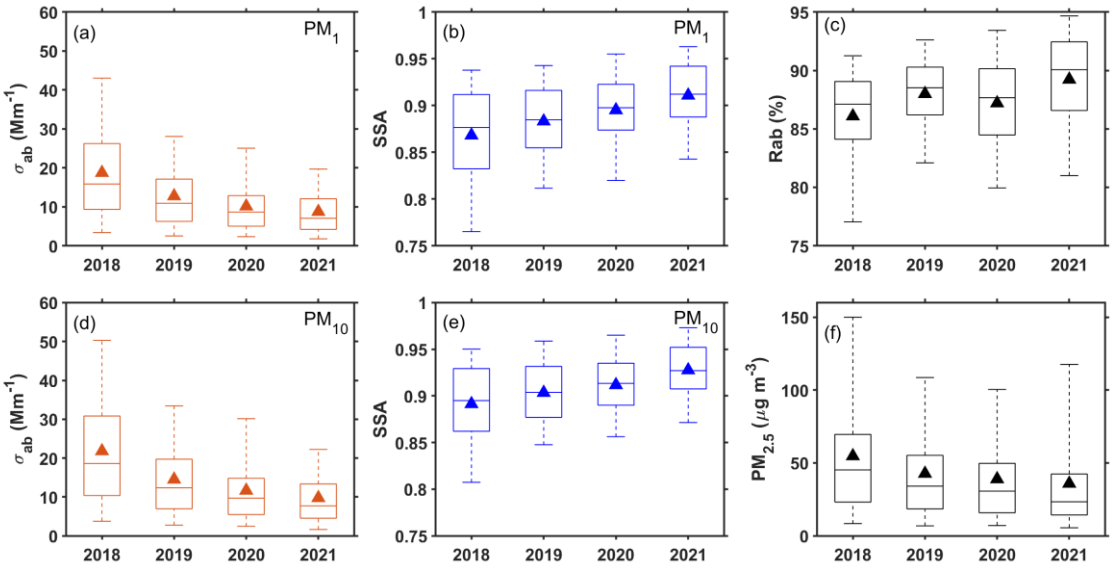

Figure 1. Annual variation of aerosol optical properties and $PM_{2.5}$ mass concentration, absorption coefficient σ_{ab} at 550 nm for (a) PM_1 and (d) PM_{10}, SSA at 550 nm for (b) PM_1 and (e) PM_{10}, (c) Rab and (f)$PM_{2.5}$ mass concentration. The solid line inside the box represents the median and the triangle indicates the mean. The box contains the range of values from 25% (bottom) to 75% (top), and the upper and lower whiskers are the 95th and 5th percentiles, respectively.

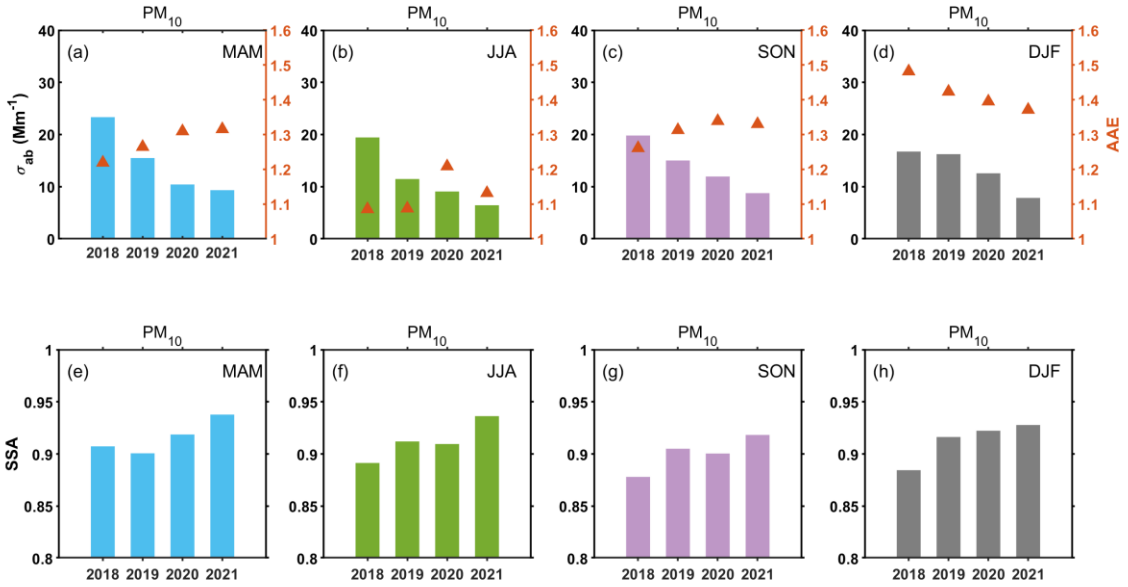

868

869 **Figure 2.** Seasonal variation of aerosol optical properties of PM_{10} from 2018-2021, (a-d)

870 σ_{ab} (bar) at 550 nm, $AAE_{450/700}$ (triangle), and (e-h) SSA (bar) at 550 nm.

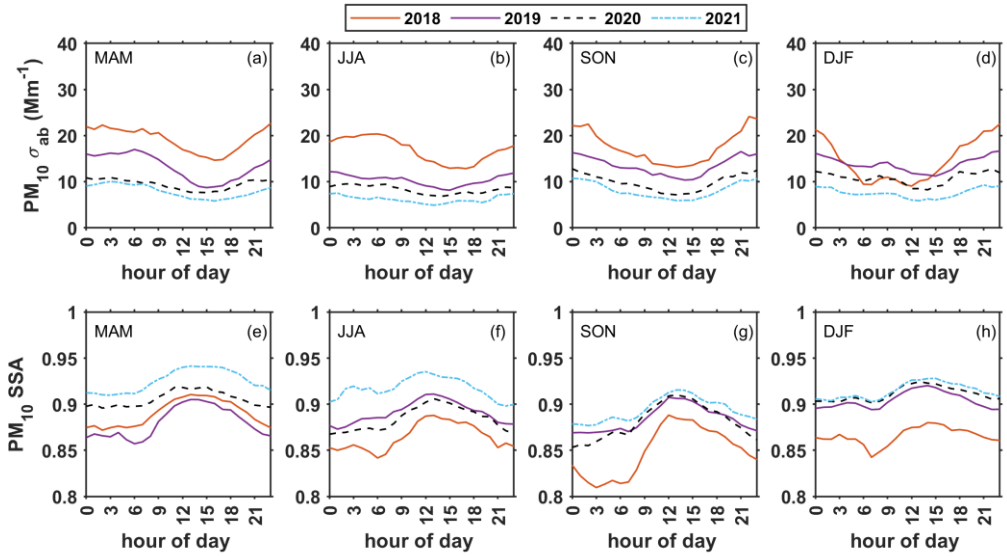

871

872 **Figure 3.** Diurnal variations of σ_{ab} (a-d) and SSA (e-h) at 550 nm for PM_{10} in four seasons

873 from 2018 to 2021.

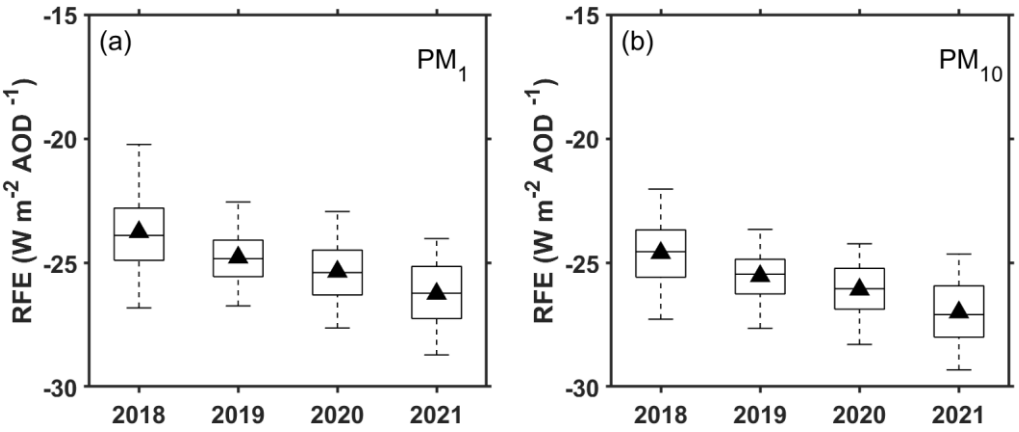

874

875 **Figure 4.** The annual variation of aerosol radiative forcing efficiency for PM_1 (a) and PM_{10}

876 (b). The solid line inside the box represents the median, and the triangle indicates the mean.

877 The box contains the range of values from 25% (bottom) to 75% (top), and the 95th and

878 5th percentiles, respectively.

879

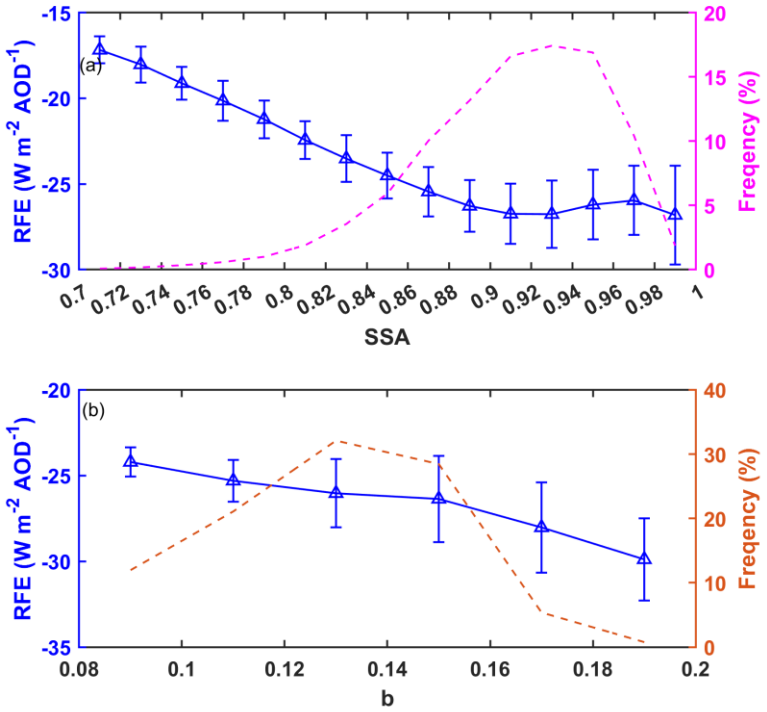

880

881 **Figure 5.** The relationship of RFE with (a) SSA and (b) backscatter fraction. The pink dash

882 line represents the frequency distribution of SSA (a) and the brown dash line represents the

883 frequency distribution of backscatter fraction (b).

884

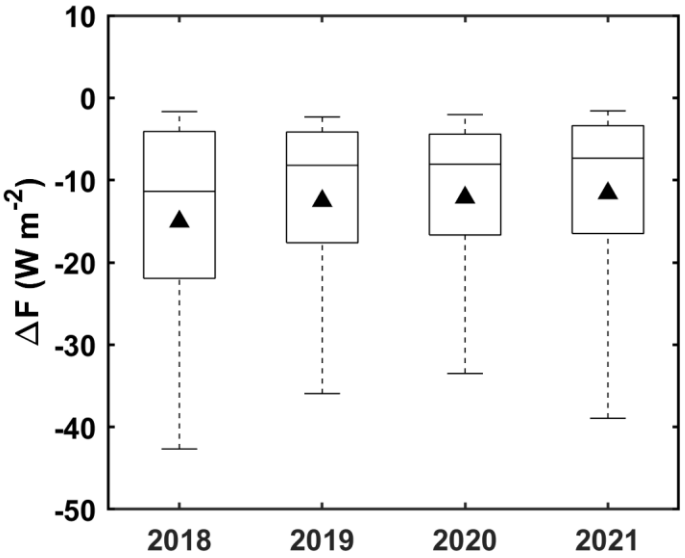

885

886 **Figure 6.** Annual variation of aerosol radiative forcing (ΔF) at TOA from 2018 to 2021
887 calculated from daily mean data. The solid line inside the box represents the median, and
888 the triangle indicates the mean. The box contains the range of values from 25% (bottom)
889 to 75% (top), and the 95th and 5th percentiles, respectively.

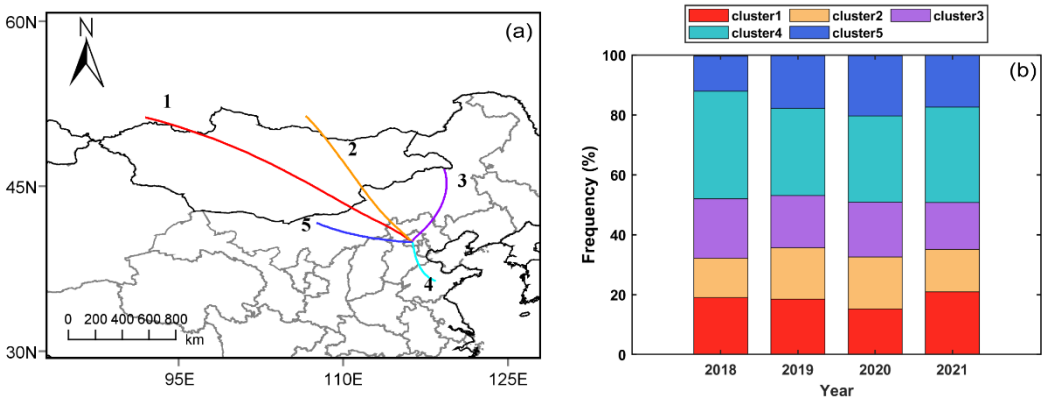

890

891 **Figure 7.** (a) Air mass clusters of back trajectories arriving in Beijing during 2018–2021
892 and (b) the fraction of each cluster accounting for the total back trajectories in each year.

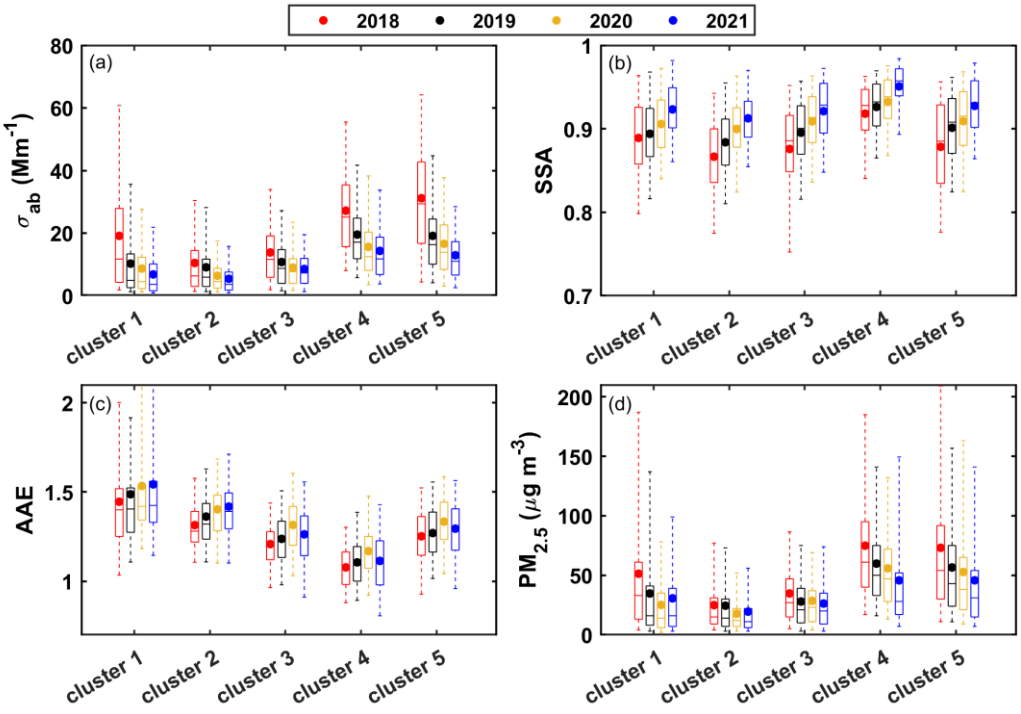

Figure 8. The variation of (a) σ_{ab}, (b) SSA, (c) AAE, and $PM_{2.5}$ mass concentration in each cluster from 2018 to 2021. The solid line inside the box represents the median and the dot indicates the mean. The box contains the range of values from 25% (bottom) to 75% (top), and the 95th and 5th percentiles, respectively.